Meta-metabolomic responses of river biofilms to cobalt exposure and use of dose-response model trends as an indicator of effects

Simon Colas, Benjamin Marie, Mathieu Milhe-Poutingon, Marie-Claire Lot, Amiel Boullemant, Claude Fortin, Séverine Le Faucheur

Journal of Hazardous Materials 470 (2024) 134099

Contents lists available at ScienceDirect

Journal of Hazardous Materials

journal homepage: www.elsevier.com/locate/jhazmat

Meta-metabolomic responses of river biofilms to cobalt exposure and use of dose-response model trends as an indicator of effects

Simon Colas [a,*], Benjamin Marie [b], Mathieu Milhe-Poutingon [a], Marie-Claire Lot [c], Amiel Boullemant [d], Claude Fortin [e], Séverine Le Faucheur [a]

[a] Universite de Pau et des Pays de l'Adour, E2S-UPPA, CNRS, IPREM, Pau, France
[b] UMR 7245 CNRS/MNHN " Molécules de Communication et Adaptations des Micro-organismes ", Muséum National d'Histoire Naturelle, Paris, France
[c] TotalEnergies, Pole d'Études et de Recherche de Lacq, France
[d] BCenv, Gardanne, France
[e] Institut National de la Recherche Scientifique – Eau Terre Environnement, Québec, Canada

HIGHLIGHTS

- Cobalt exposure reduces biomass and chlorophyll content in biofilms.
- Cobalt exposure alters the meta-metabolomic fingerprint of biofilms.
- Meta-metabolomic defense responses are characterized by biphasic trends.
- Meta-metabolomic damage responses are characterized by monotonic trends.
- Trend analysis of metabolite dose-response curves is a promising avenue for omics.

GRAPHICAL ABSTRACT

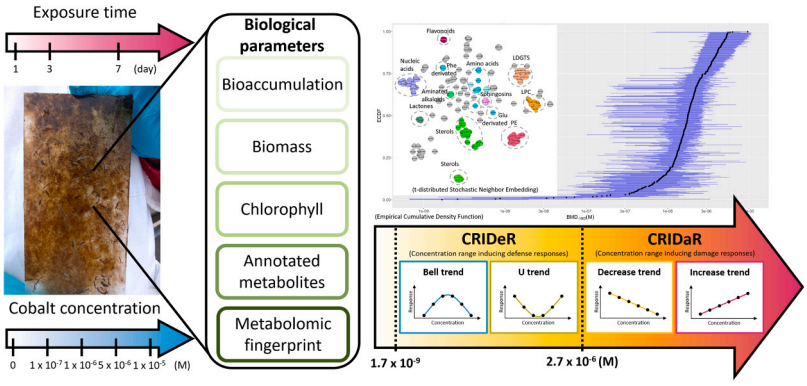

ARTICLE INFO

Keywords:
Metals
Microbial ecotoxicology
Benchmark-doses
Metabolites
Microcosms

ABSTRACT

The response of the meta-metabolome is rarely used to characterize the effects of contaminants on a whole community. Here, the meta-metabolomic fingerprints of biofilms were examined after 1, 3 and 7 days of exposure to five concentrations of cobalt (from background concentration to 1×10^{-5} M) in aquatic microcosms. The untargeted metabolomic data were processed using the DRomics tool to build dose-response models and to calculate benchmark-doses. This approach made it possible to use 100% of the chemical signal instead of being limited to the very few annotated metabolites (7%). These benchmark-doses were further aggregated into an empirical cumulative density function. A trend analysis of the untargeted meta-metabolomic feature dose-response curves after 7 days of exposure suggested the presence of a concentration range inducing defense responses between 1.7×10^{-9} and 2.7×10^{-6} M, and of a concentration range inducing damage responses from

Abbreviations: BMD, benchmark-dose; BMR, benchmark-response; CRIDaR, concentration range inducing damage responses; CRIDeR, concentration range inducing defense responses; EC_x, effective concentration; ECDF, empirical cumulative density function; LC-HRMS, liquid chromatography-high resolution mass spectrometry.

* Corresponding author.
E-mail address: simon.colas@univ-pau.fr (S. Colas).

https://doi.org/10.1016/j.jhazmat.2024.134099
Received 14 November 2023; Received in revised form 18 March 2024; Accepted 19 March 2024
Available online 20 March 2024

2.7×10^{-6} M and above. This distinction was in good agreement with changes in the other biological parameters studied (biomass and chlorophyll content). This study demonstrated that the molecular defense and damage responses can be related to contaminant concentrations and represents a promising approach for environmental risk assessment of metals.

1. Introduction

In aquatic ecosystems, biofilms grow on submerged substrata and form the basis of the aquatic food web, as they include a large proportion of primary producers (algae and cyanobacteria) as well as bacteria, fungi and meiofauna. These communities are well known to accumulate metals as a function of their ambient concentration and speciation [1–3]. Effects of metals on biofilms have been shown at all levels of biological organization, from subcellular [4,5] and cellular [6–9] levels to communities [4,5,10]. Among these effects, modification of metabolite contents can be linked to stressors [11]. Metabolites are low molecular-weight molecules produced during metabolism with various cellular roles in basal functioning and defense mechanisms [11], such as in osmoregulation, antioxidant activities or metal chelation [12]. They can also be related to damages caused by stress such as lipid peroxidation [13] or hypoxia [14].

Examination of a whole metabolome is commonly referred to as metabolomic fingerprinting [15] and is often conducted using untargeted Liquid Chromatography-High Resolution Mass Spectrometry (LC-HRMS) [16]. The strength of the untargeted meta-metabolomics approach is based on the absence of an a priori assumption for the type and function of molecules required prior to analysis, thus broadening the potential number of compounds that could be characterized. In this approach, both unannotated and annotated metabolites are considered; the annotation consisting of assigning a tentative metabolite candidate from a set number of identified compounds within a database on its mass, its retention time and its spectral fragmentation. However, metabolite annotation is database-dependent and to this date, only a small portion of the metabolomic fingerprint can be identified [17], typically only 4 to 5% [18]. Using only the annotated metabolites therefore results in the loss of a significant part of the chemical information acquired through untargeted analysis. The processing of metabolomics data is often restricted to multivariate statistical approaches in order to distinguish control groups from groups exposed to contaminants [19]. Although less frequently used, dose-response curves can also be drawn using the metabolite response. As such, benchmark doses (BMDs) can be extracted, which correspond to the doses of the tested contaminants at which the response of the exposed organisms differs from the control group [15,20,21]. These BMDs can be further aggregated in an empirical cumulative density function (ECDF) to get the whole metabolome response as a function of the contaminant exposure concentration [15,22]. Building metabolite ECDFs for biofilms exposed to contaminants such as metals may therefore provide valuable information on their exposure and effects.

Apart from ECDFs, dose-response curves for metabolomic response as a function of concentration may be further used by examining their trends. Indeed, one of our recent meta-analysis conducted on 2595 dose-response curves described by defense and damage biomarkers in 18 phyla exposed to inorganic and organic contaminants demonstrated that defense biomarkers mainly describe biphasic responses (bell- and U-shaped trends) whereas damage biomarkers mainly follow monotonic responses (decreasing and increasing trends) [23]. As such, cellular defense mechanisms such as the activities of antioxidant enzymes [24,25], phytochelatins [26] or biotransformation enzymes and associated compounds [26] preferentially describe a bell-shaped or U-shaped trend. On the other hand, cellular damage mechanisms such as change in pigment content [24,25], reactive oxygen species [24] or malonaldehyde levels [27] preferentially vary in a monotonical way via increasing or decreasing trends [23]. In other words, the induction of a defense mechanism, the role of which is to have a positive impact on the organism, would begin following exposure to low-level stress up to a certain threshold of intensity from which the organisms' defense mechanisms are overwhelmed. The concentrations of the metabolites involved in a defense response would then decrease [28], explaining a bell-shaped response. The U-shaped dose-response would follow the same biphasic response principle [28]. For damages linked metabolites, their induction would mainly be initiated once the defense mechanisms have been overcome and would result from the continuous degradation of cellular and sub-cellular compounds, hence their tendency to increase and decrease in proportion to the intensity of the stress [29].

The objective of the present study was to couple the use of ECDFs constructed with BMDs with the analysis of dose-response trends. We aimed to develop a robust novel approach to assess metal effects on biofilms based on 100% of the measured untargeted metabolomic signal without restricting ourselves to limited pool of annotated metabolites. Our hypothesis, based on our aforementioned meta-analysis [23], is that the dose-response curve trends (biphasic or monotonic) of untargeted meta-metabolomic features allow us to determine the stress state (defense or damage) of organisms.

Cobalt (Co) was selected as the metal of interest as it is considered an emerging contaminant due to the current energy transition from fossil fuels to decarbonized energy, which requires intensive use of Co-containing batteries [30,31]. Cobalt has recently been identified as a relevant substance to be monitored in France [32] and as a toxic substance in Canada [33]. Its effects on microorganism communities has been poorly studied, which limits the capacity of environmental regulators to adequately conduct a thorough risk assessment [34–37].

In this work, mature river biofilms were exposed for 7 days to increasing Co concentrations in microcosms. Cobalt bioaccumulation, biomass, chlorophyll content and meta-metabolome response were determined. Both endogenous metabolites (contained within organisms or adsorbed on their surface) and exogenous metabolites (excreted by organisms) were included. The relevance of the calculated concentration range inducing defense responses (CRIDeR) and concentration range inducing damage responses (CRIDaR) based on the trends of untargeted meta-metabolomic feature dose-response curves (Fig. S1) was assessed by comparing their range of induction with biomass and chlorophyll content.

2. Material and methods

2.1. Biofilm colonization and exposure to Co in microcosms

Biofilm colonization and exposure experiments were carried out at the outdoor TotalEnergies facility (pilot rivers) in Lacq (France). Four weeks before the start of the experiment, the mature biofilms were collected by natural colonization of glass slides (5 × 10 cm). A total of 15 microcosms were filled with 15 L of river water (Gave de Pau, France); three for each of the five Co exposure conditions: 2×10^{-9} M (river background Co concentration used as control), 1×10^{-7}, 1×10^{-6}, 5×10^{-6} and 1×10^{-5} M Co. Cobalt (Standard solution, 1000 mg Co·L^{-1}, Supelco, Germany) was added to each microcosm and left to equilibrate for 24 h. The microcosms were placed in one of the artificial streams of the facility in order to maintain the water temperature at 13.5 ± 1.0 °C (Table S1). Seven mature biofilm slides were placed in each microcosm (105 in total). After one, three and seven days of exposure (D1, D3 and D7), two biofilm slides were collected from each microcosm, one for Co accumulation and one for meta-metabolomics. At D7, one additional

slide was sampled for the determination of chlorophyll content. The samples were stored in the dark at −20 °C before analysis. The preparation of exposure media is further described in the Supplementary material (Text S1).

2.2. Water analysis and Co speciation

At D−1, D1, D3 and D7, triplicate samples (10 mL) of exposure medium were collected from each microcosm to determine metal concentrations. Samples for cation, anion and dissolved organic carbon concentrations were collected at D−1. The sampling and analysis protocol of the different physicochemical parameters of the exposure media are presented in Text S2.

2.3. Biofilm analysis

Biofilm samples collected for the determination of Co accumulation, chlorophyll content and meta-metabolome analysis were freeze-dried (CRIOS-80, Cryotec, France) and weighed prior to further processing. These data were used to express the quantity of dry biomass (in g) per glass slide area (cm^2), referred to as "biomass" in the remainder of the manuscript. To obtain total and intracellular Co concentrations, the freeze-dried biofilms were digested with 70% HNO_3 acid and 30% H_2O_2 before being mineralized (UltraWAVE™ oven, Milestone, Italy). To distinguish between total and intracellular Co content, biofilms were previously rinsed with 10 mM ethylenediaminetetraacetic (EDTA) for 10 min in order to remove adsorbed metals on the biofilm surface [1, 38]. Metal concentrations were measured by inductively coupled plasma mass spectrometry (model 7500, Agilent, CA, USA). The detailed protocol for the determination of bioaccumulated Co is provided in Text S3. Chlorophyll content was analyzed by spectrophotometry with different pigments (chlorophyll a, chlorophyll b and chlorophylls c1 and c2) quantified using the Jeffrey and Humphrey protocol [39], with further details presented in Text S4. Meta-metabolomic analyses were carried out at the *Muséum national d'Histoire naturelle* (Paris, France) following the method of Le Moigne et al. [40]. Briefly, freeze-dried biofilms (1 mg) were diluted in 10 µL of cold 75% methanol acidified with 0.1% formic acid and sonicated on ice for 30 s, at 80% of the maximum intensity (SONICS Vibra Cell, Newton, CT, USA; 130 Watts, 20 kHz), with the homogenates then centrifuged at 4 °C (12,000 g: 10 min). The supernatants were then collected and stored in the dark at −20 °C. For the mass spectrometry analysis, 2 µL of the extracts were injected into an ultra-high-performance liquid chromatography instrument (ELUTE, Bruker, Bremen, Germany) equipped with a Polar Advance II 2.5 pore C18 (Thermo Fisher Scientific, Waltham, MA, USA) chromatographic column. The molecule separation was obtained with a flow rate of 300 $\mu L \cdot min^{-1}$ under a linear gradient of acetonitrile (from 5 to 90% in 15 min) acidified with 0.1% formic acid. Metabolite contents were then determined using an electrospray ionization hybrid quadrupole time-of-flight high-resolution mass spectrometer (Compact, Brucker, Bremen, Germany) in the range of 50–1500 *m/z*. The global feature contents were extracted from raw data with Metaboscape 4.0 (Bruker) and annotation was attempted by molecular network approach performed with MetGem 1.3.6. The analysis method and annotation protocol are detailed in Text S5. Raw LC-HRMS data are available at the National Institutes of Health Common Fund's National Repository website and the Metabolomics Workbench [41] (https://www.metabolomicsworkbench.org) with the assigned Project ID PR001754. The data can be accessed directly via its Project DOI: https://doi.org/10.21228/M8071P.

2.4. Construction of dose-response models and ECDF

Dose-response curves were built based on the biofilm meta-metabolomic response to Co^{2+} concentrations at D7 using the DRomics package in R software following the recommendations of the European Food Safety Authority Scientific Committee and those of Larras et al. [20,21]. Pre-processing was performed on the raw LC-HRMS data. First, the half-minimum method was applied for missing values. The data set was then log-2 transformed and the significantly responding untargeted meta-metabolomic features were selected using an ANOVA with a false discovery rate of 0.05. For each selected untargeted meta-metabolomic feature, dose-response models (linear, Hill, exponential, Gauss-probit or log-Gauss-probit) were then fitted by non-linear regression. The model with the lowest second-order Akaike information criterion value was chosen. When dose-response curves could not be reliably fitted, the untargeted meta-metabolomic feature was removed from the analysis. The models were further characterized according to their trends (bell-shaped, decreasing, increasing and U-shaped) of the fitted dose-response curves.

Once the best dose-response models were constructed for each untargeted meta-metabolomic feature previously selected, a BMD_{-1SD} was calculated from a benchmark-response (BMR_{-1SD}) using the following equation (Fig. 1):

$$BMR_{-zSD} = y0 \pm z \times SD$$

where y0 is the mean control response (average concentration of the untargeted meta-metabolomic feature detected in the biofilms of the control group), SD is the residual standard deviation of the considered model, *i.e.*, 95% confidence interval and z is the factor of SD (z fixed at 1, a value proposed by the European Food Safety Authority) [15]. In other terms, BMR_{-1SD} defines the first value of the response of exposed biofilms that differs from that of control biofilms, and BMD_{-1SD} is the Co concentration at which this BMR_{-1SD} occurs. When the calculated BMR_{-1SD} was within the range of response values defined by the model but the corresponding BMD_{-1SD} value was calculated to be outside the range of the tested Co concentrations, the untargeted meta-metabolomic feature was not taken into account (Fig. 1). The confidence interval on the BMD_{-1SD} values were calculated by bootstrapping (1000 iterations). After this step, models were removed when one of the bounds of their 95% confidence interval could not be computed. Such a result could be obtained when bootstrapped BMD_{-1SD} values were not reachable due to model asymptotes or to calculated values outside the range of tested doses.

Finally, the distribution of all $BMDs_{-1SD}$ was compiled into an empirical cumulative density function (ECDF) also built with the DRomics R package to obtain an integrative response of biofilm exposure. The ECDF is a step function that jumps up by 1/N at each of the N data points from the untargeted meta-metabolomic with the lowest BMD_{-1SD} to the untargeted meta-metabolomic feature with the highest BMD_{-1SD}. Additional ECDFs were further constructed as a function of the dose-response curve trends.

2.5. Statistical treatments

The significance of Co exposure on Co bioaccumulation, biomass and chlorophyll content was assessed according to Dunn's *post-hoc* test after Kruskal-Wallis non-parametric tests on R software. Analyses of unannotated and annotated metabolites were performed on MetaboAnalyst 5.0, including matrix normalization (Pareto), partial least square discriminant analysis and ANOVA (analysis of variance).

3. Results

3.1. Characterization of the Co concentration in the exposure media

The river water used for exposure media preparation, had background total dissolved concentrations of $1.7 \pm 0.2 \times 10^{-9}$ M Co, $4.1 \pm 0.1 \times 10^{-5}$ M Ca, $2.9 \pm 0.1 \times 10^{-6}$ M Mg, 1.2 ± 0.3 mg $C \cdot L^{-1}$ and a mean pH of 7.90 ± 0.02 (Table S2). Cobalt was predicted to be mainly present in its free form Co^{2+} (65%), and the remaining species being

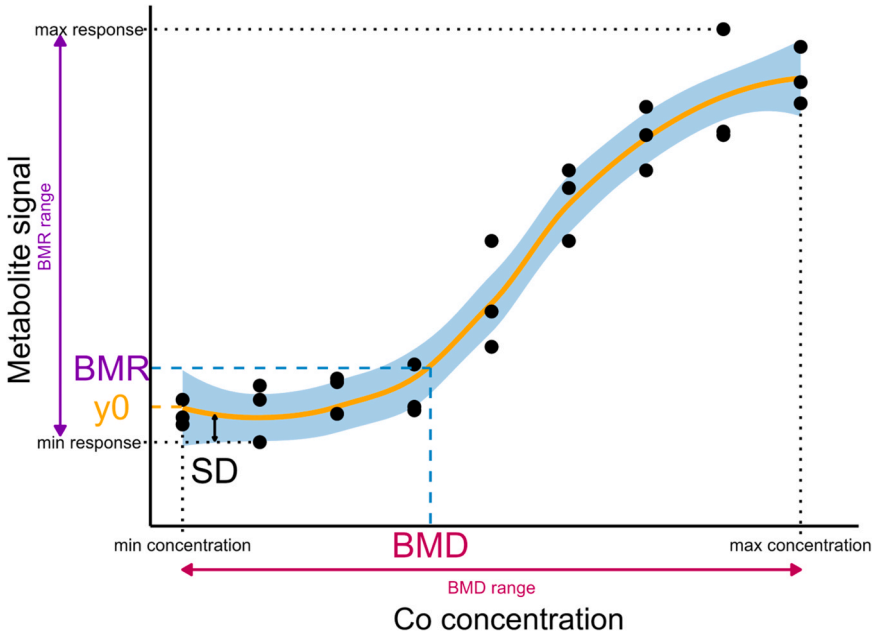

Fig. 1. Schematic illustration of a benchmark-dose calculation for one studied untargeted meta-metabolomic feature. The black dots represent measured MS peak intensities of the studied untargeted meta-metabolomic feature after pre-processing. The orange line is the constructed dose-response curve (model) from the measured peak intensities as a function of exposure Co concentrations. The blue area represents the 95% confidence intervals of the model (or the residual standard deviations of the model, SD). The mean control response is y0 and is used with the standard deviation (SD) to define the benchmark-response (BMR). The Benchmark-Dose (BMD) is then calculated from the BMR.

mostly present as carbonato-complexes, $CoCO_3$. A small percentage of the total Co (< 0.01%) was calculated to be bound by fulvic acid. The average total dissolved Co concentration, taking into account the three sampling days (D1, D3 and D7) for each exposure condition were $3.1 \pm 1.8 \times 10^{-9}$, $1.4 \pm 0.8 \times 10^{-7}$, $1.6 \pm 0.8 \times 10^{-6}$, $8.6 \pm 3.7 \times 10^{-6}$ and $1.6 \pm 0.7 \times 10^{-5}$ M, respectively (Table S1). The corresponding calculated average Co^{2+} concentrations were $1.5 \pm 0.9 \times 10^{-9}$, $0.7 \pm 0.6 \times 10^{-7}$, $0.7 \pm 0.5 \times 10^{-6}$, $4.0 \pm 0.9 \times 10^{-6}$ and $0.8 \pm 0.2 \times 10^{-5}$ M, respectively (Table S1).

3.2. Metal bioaccumulation

Mature biofilms naturally contained $1.3 \pm 0.1 \times 10^{-7}$ mol·g^{-1} Co (Table S3). Cobalt intracellular contents significantly increased with exposure concentrations (Fig. 2A and Table S3) at each sampling time (D1, D3 and D7). After D7, the majority of accumulated Co by biofilms was found to be intracellular (70 ± 20%; n = 15). Background intracellular Co concentration was $1.23 \pm 0.08 \times 10^{-7}$ mol·g^{-1}. Both total and intracellular Co accumulation were significantly correlated with total dissolved Co and free Co^{2+} concentrations in the exposure media (Fig. S2 and Table S3). The description of the obtained correlations between Co concentrations in exposure media and accumulated by biofilms are presented in Text S6. The accumulation of other metals (Li, Ni, Cu, Zn, Pb, As and Cd) naturally present in the exposure media was not impacted by exposure to Co (Table S3).

3.3. Biomass

Biofilms exposed to natural background concentrations of Co and exposed to 1×10^{-7} and 1×10^{-6} M Co presented similar biomass throughout the whole duration of the experiment (Fig. 2B). In contrast, biofilm biomass significantly decreased from D3 when they were exposed to 5×10^{-6} M Co. This decrease was accentuated at D7 for biofilms exposed to the highest Co concentrations (5×10^{-6} and 1×10^{-5} M). The greatest effect was observed at the concentrations of 5×10^{-6} and 1×10^{-5} M Co, concentrations at which the biomass decreased by 83% (from 80 to 13 mg·cm^{-2}) and 69% (77 to 24 mg·cm^{-2}), respectively.

3.4. Chlorophyll content

Lower chlorophyll *a*, *b* and $c_1 + c_2$ contents at D7 were observed with increasing Co concentrations (Fig. 2C). At the end of the experiment, biofilms exposed to natural Co concentrations had a total chlorophyll content of 0.73 µg·cm^{-2}, while those exposed to the two highest concentrations had 0.10 and 0.15 µg·cm^{-2} of chlorophyll, respectively. After a week of exposure, the highest Co concentrations (5×10^{-6} and 1×10^{-5} M) led to a decrease in chlorophyll content of up to 85%.

At D7, the relative composition of the different chlorophyll pigments was significantly different at the highest Co concentration compared to the control, 1×10^{-7} and 1×10^{-6} M Co exposure conditions (Fig. 2D). Although the relative contents of chlorophylls *a* and $c_1 + c_2$ were not significantly modified in biofilms exposed to 1×10^{-5} M, with respect to the control, the relative content of chlorophyll *b* was 5.5-fold higher.

3.5. Meta-metabolomic response

In total, 2117 untargeted meta-metabolomic features were observed (Table S4) among all samples and 159 of them were annotated, representing 7.5% of the whole metabolomic fingerprint. Attempts were made to identify different families of molecules, including several lipids or lipid precursors (lyso-diacylglyceryltrimethylhomoserine, sterol, phosphatidylethanolamine, lysophosphatidylcholine, sphingosines) (Fig. 3 and Fig. S3). The biofilm meta-metabolomic response was examined by comparing the samples at each exposure Co concentration and each exposure time, first for the whole 2117 untargeted meta-metabolomic features and second using the 159-annotated metabolite datasets.

3.5.1. Using all untargeted meta-metabolomic features

Cobalt concentrations in the exposure media significantly impacted the levels of 489 untargeted meta-metabolomic features and the

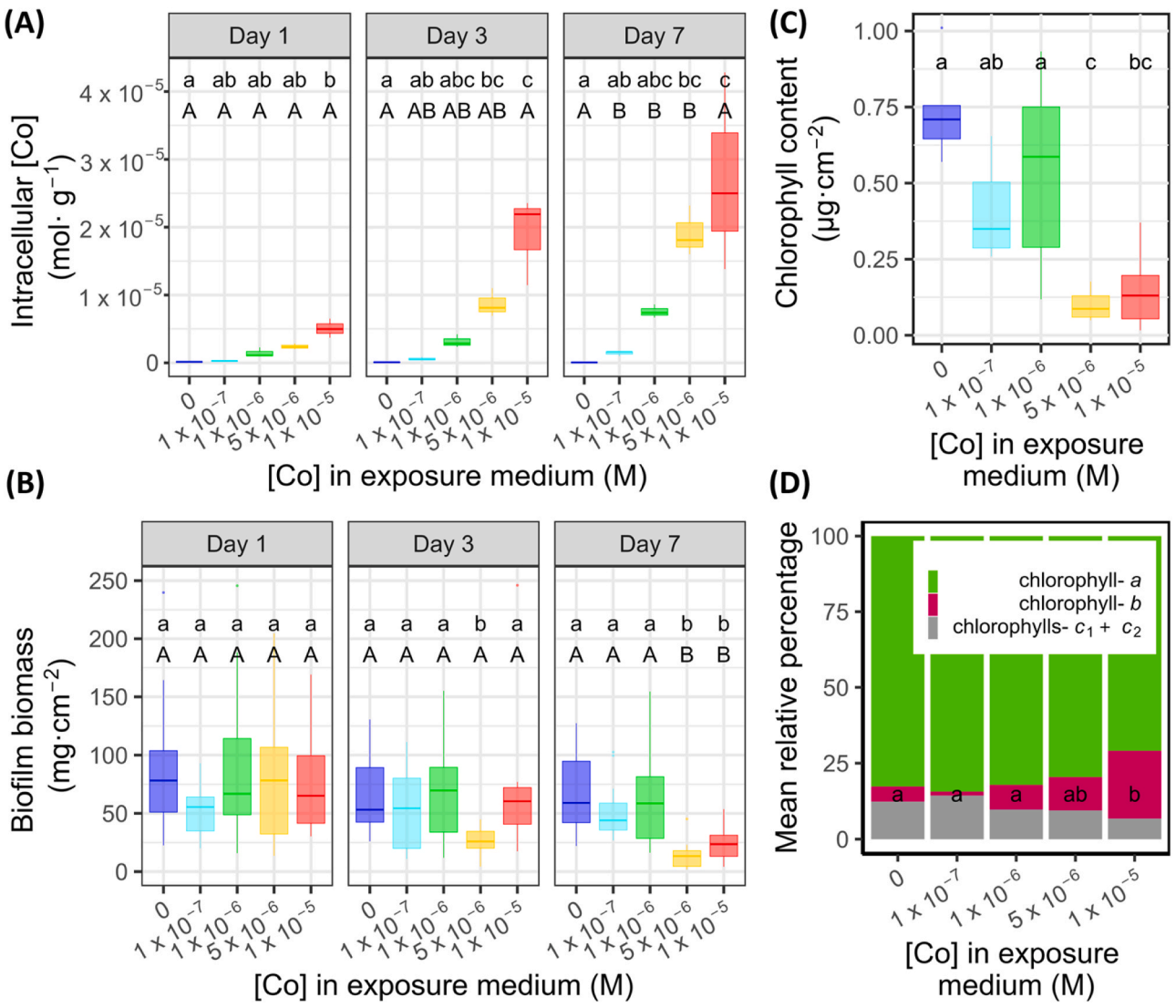

Fig. 2. Accumulation and effects of Co on biomass and chlorophyll contents of river biofilms. (A) Intracellular Co content (mol·g^{-1}) as a function of total Co concentration in the exposure medium (M) over time (in days). (B) Biofilm biomass (mg·cm^{-2}) over time (in days) according to Co exposure concentrations (M). (C) Chlorophyll contents (µg·cm^{-2}) after 7 days of exposure as a function of exposure concentration Co (M). (D) Mean relative percentage of pigment composition in chlorophylls of biofilms exposed for 7 days to different Co concentrations. The lower-case letters correspond to the significative groups defined by a Dunn's *post-hoc* test ($p < 0.05$) performed after Kruskal-Wallis non-parametric tests among Co exposure concentrations at each exposure time and the capital letters correspond to the significant groups defined by a Dunn's *post-hoc* test ($p < 0.05$) performed after Kruskal-Wallis non-parametric tests among the exposure times for each exposure concentration.

exposure time affected 522 untargeted meta-metabolomic features. The interaction of the two factors induced the modification of 502 untargeted meta-metabolomic features (two-way ANOVA; $p < 0.05$). In total, out of 2117 untargeted meta-metabolomic features observed, 1513 of them show relative content variations (Fig. S4), which represents more than 71% of the whole meta-metabolome that could be detected.

The effects of Co and exposure time on meta-metabolomic response were investigated using supervised partial least-squares discriminate analysis. These showed significant R^2 *cumulative*, Q^2 *cumulative* (Table S5) and permutation scores (0/2000 permutations; $p < 0.0005$). The meta-metabolomic response of the control biofilms did not vary between D1 and D3 (Fig. 4A). However, at D7, a significant difference was observed compared to D1 and D3 (PERMANOVA; $p < 0.05$) (Fig. 4A). At D1, the global meta-metabolomic signature was only different between biofilms exposed to 1×10^{-7} and 1×10^{-5} M Co (PERMANOVA; $p < 0.05$) (Fig. 4B). At D3, the meta-metabolomic signature between control biofilms was different from those of biofilms exposed to 5×10^{-6} and 1×10^{-5} M Co (PERMANOVA; $p < 0.05$). In addition, the signature of biofilms exposed to 1×10^{-7} M Co differed from that of biofilms exposed to 1×10^{-5} M, but not to those of biofilms exposed to the other studied concentrations (PERMANOVA; $p < 0.05$). The metabolic profile of biofilms exposed to 5×10^{-6} M Co was also different from biofilms exposed to 1×10^{-5} M (PERMANOVA; $p < 0.01$) (Fig. 4C). At D7, the meta-metabolomic response was different among all the studied exposure concentrations, except for the control biofilms and those exposed to 1×10^{-7} M Co (PERMANOVA; $p < 0.05$) (Fig. 4D). Finally, for each exposure condition, the meta-metabolomic signature of the biofilms was different between D1 and D7 (PERMANOVA; $p < 0.05$). The differences and the similarities in the biofilm meta-metabolomic profiles can also be observed on a heatmap with hierarchical classification representation (Euclidean distance, Fig. 4E). The profiles of the control biofilms (at each time step), and those of the biofilms exposed to the lowest Co concentration at D1 are gathered in the same group. The meta-metabolomic profiles of the biofilms exposed to the two highest Co concentrations at D7 were also grouped together.

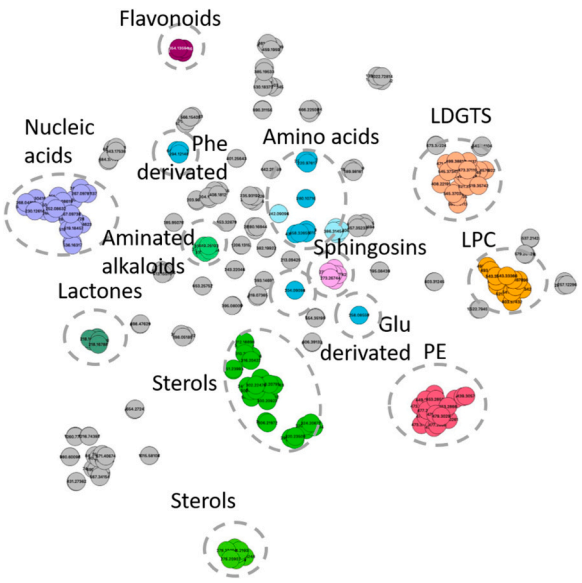

Fig. 3. T-*SNE* molecular network generated with Metgem 1.3.6 based on LC-MSMS dataset obtained for all samples. The various colors show the different molecular families that constitute the different annotated clusters according to molecular fragment similarities with standards available in public database (GNPS, HMDB, NIH and EMBL).

3.5.2. *Using only annotated metabolites*

Similar results were observed for the annotated metabolites (159 untargeted meta-metabolomic features) whose detailed analysis is presented in Text S7, Fig. 3 and Fig. S3. Cobalt concentrations in the exposure media significantly induced a change in the production of 39 annotated metabolites. Over the exposure time, the content of 25 annotated metabolites were disrupted whereas the interaction of the two factors impacted the content of 33 metabolites (two-way ANOVA; $p < 0.05$). Overall, 61% of the biofilm metabolites were disturbed by the experimental treatments. A closer look at the meta-metabolomic profiles (Fig. S3G and Fig. S3H) showed that exposure to Co caused a modification in the production of certain nucleic acids and amino acids, and in particular a greater production of lipid and lipid precursors as well as a decrease in the flavonoid content.

3.5.3. *Dose-response models*

Dose-response curves were constructed to illustrate meta-metabolome response as a function of Co concentrations at D7. Out of 2117 untargeted meta-metabolomic features, 892 untargeted meta-metabolomic features were selected using an ANOVA with a false discovery rate of 0.05. Using the Akaike information criterion to select the best fit models, 236 dose-response curves out of these 892 curves were removed as no model could be reliably fitted. From the remaining modelled dose-response curves, three BMD_{-1SD} values could not be calculated as the BMR stands within the range of response values defined by the model but outside the range of tested doses. Also, bootstrap confidence interval computation failed on eight untargeted meta-metabolomic features due to the lack of convergence of the model fit for a fraction of the bootstrapped sampled greater than 0.5.

Benchmark-doses ($BMDs_{-1SD}$) calculated from each fitted dose-response curve were grouped together via ECDF (Fig. 5A and Table S6). Out of 656 BMD_{-1SD} values, 167 were removed because at least one bound of the 95% confidence interval could not be computed due to bootstrapped BMD_{-1SD} values which could not be reached. With respect to control conditions, 2% of the untargeted meta-metabolomic features were impacted at 1×10^{-7} M Co, an additional 15% at 1×10^{-6} M, another 78% at 5×10^{-6} M, while the remaining 5% of untargeted meta-metabolomic features were impacted at the highest Co concentration tested (1×10^{-5} M).

The models were further classified into four different categories as a function of their respective curve trend: 151 exhibited a bell-shaped curve, 92 an increasing trend, 121 a decreasing trend and 117 a U-shaped curve (Fig. 5B and Table S6). Using the ECDF curve, two main Co concentration ranges of meta-metabolomic response could be distinguished based on the inflection point (point where the second derivative of the ECDF has changed sign) of the $BMDs_{-1\ SD}$ distribution: the first one ranging from 1.7×10^{-9} to 2.7×10^{-6} M of added Co^{2+} and the second from 2.7×10^{-6} M of added Co^{2+} to the highest concentration (Fig. 5A). In the first concentration range, 99% of untargeted meta-metabolomic features describing a bell-shaped response curve were present and 1% in the second concentration range. For those describing a U-shaped response curve, 97% were present in the first concentration range and 3% in the second concentration range. Regarding the untargeted meta-metabolomic features with an increasing response curve, they were equally distributed (50/50) among both concentration ranges. Finally, 40% of the untargeted meta-metabolomic features with a decreasing response curve were present in the first concentration range, and 60% in the second range. (Fig. 5 and Table S6). The proportion of untargeted meta-metabolomic features with a biphasic trend (bell-shaped and U-shaped dose-response trends) was significantly greater in the first concentration range than in the second (Pearson's χ^2 test with Yates' continuity correction: $\chi^2 = 171.6$, d.f. $= 1$, $p = 3.3 \times 10^{-39}$). Conversely, the proportion of untargeted meta-metabolomic features with a monotonic trend (increasing and decreasing dose-response trends) was significantly greater in the second range than in the first range (Pearson's χ^2 test with Yates' continuity correction: $\chi^2 = 171.6$, d.f. $= 1$, $p = 3.3 \times 10^{-39}$).

Dose-response curves were also constructed to illustrate meta-metabolome response as a function of Co concentrations at D1 and D3 (Text S8). At D1, no concentration ranges of meta-metabolomic response could be distinguished, mostly due to the lower number of modelled metabolite response (20 as compare to 481 at D7) (Fig. S5). In contrast, similar concentration ranges were found at D3 as D7 (Fig. S6B). The first concentration range was between 3.1×10^{-8} and 2.1×10^{-6} M of added Co^{2+} and the second from 2.1×10^{-6} M of added Co^{2+} to the highest concentration at D3.

4. Discussion

4.1. *Effect of Co concentration and exposure time on untargeted meta-metabolome response*

Bioaccumulation must first occur before an effect can be observed. As expected, Co accumulation increased linearly as a function of the calculated free ion concentration of Co^{2+} (Fig. S2). Published laboratory and field data on Cu, Zn, Cd and Ni accumulation in biofilms have shown similar linear correlations [1–3,42]. Such net metal accumulation, visible from day 1, results from uptake and release processes [1].

Although Co contents were significantly higher in Co-exposed biofilms than in control biofilms at D1, no statistical difference was observed within their meta-metabolome (Fig. 2A and Fig. 4B). Changes to metabolites have been reported to occur within minutes after a contaminant exposure, with individual compounds identified from detoxification and damage processes [43,44]. For example, microalgae exposed to Cu, Cd and Pb enzymatically produced metal-binding phytochelatins within the first 15 min of exposure [45,46]. Using targeted metabolomic fingerprints, microalgae exposed to silver nanoparticles (97 metabolites studied) [47] and Hg (93 metabolites studied) [48] were shown to respond within 2 h. Changes in the untargeted meta-metabolome (2117 untargeted meta-metabolomic features studied in this experiment) over time in a whole microbial community, such as freshwater biofilms, has so far received little attention. A set of metabolites inherently describes a greater diversity in terms of toxicological response typology and intensity than for a single metabolite. Measuring

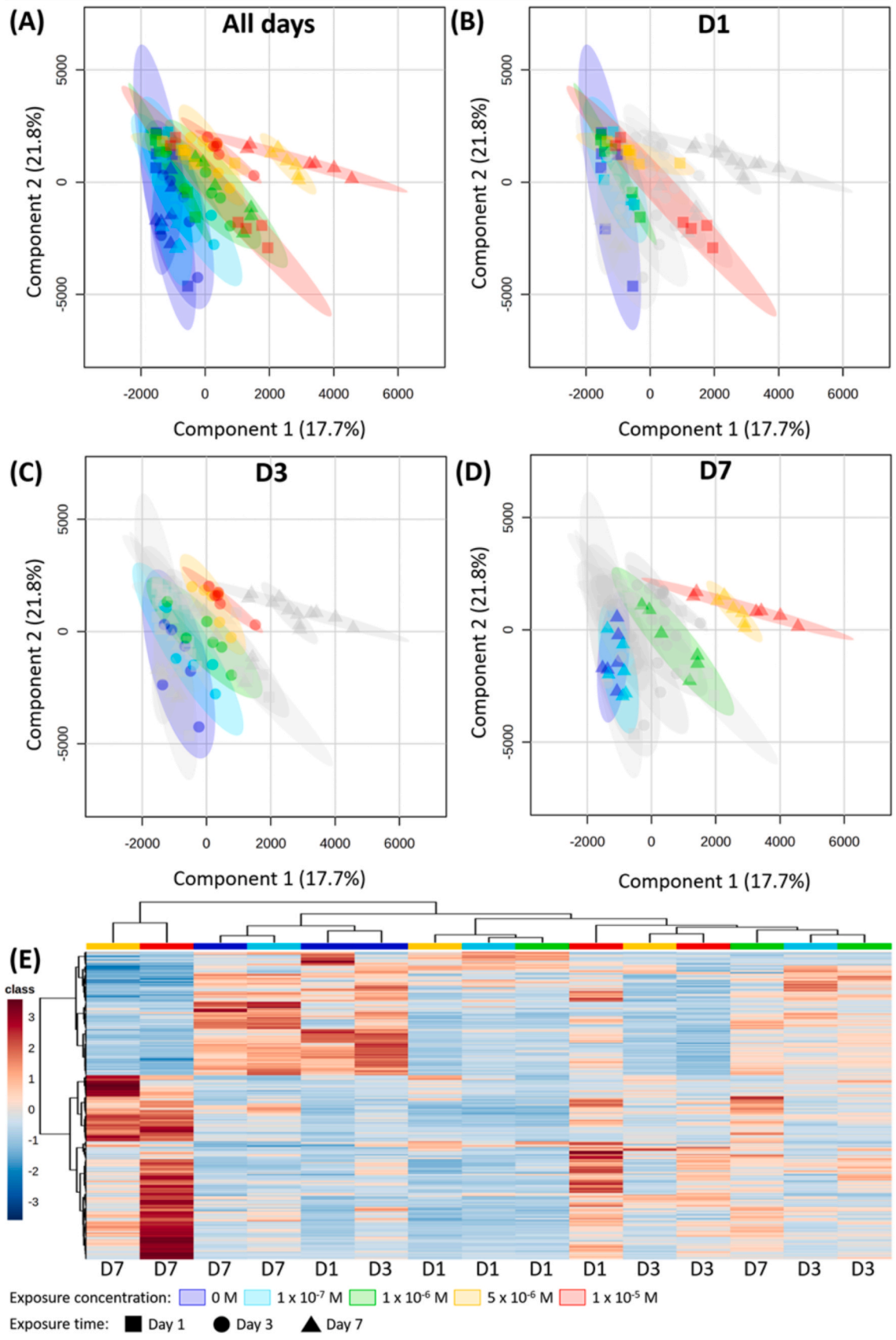

Fig. 4. Meta-metabolomics response of biofilms according to time and concentrations of exposure to Co. (A) Individual score plot generated from partial least-squares discriminate analysis performed with 2117 variables to components 1 and 2 with all conditions grouped together, after one (B), three (C) and seven (D) days of exposure. (E) Heatmap with hierarchical classification representation of concentration class averages (Ward clustering according to Euclidian distances) performed from relative intensities of the dysregulated analytes with a variable importance in projection score > 1 for component 1.

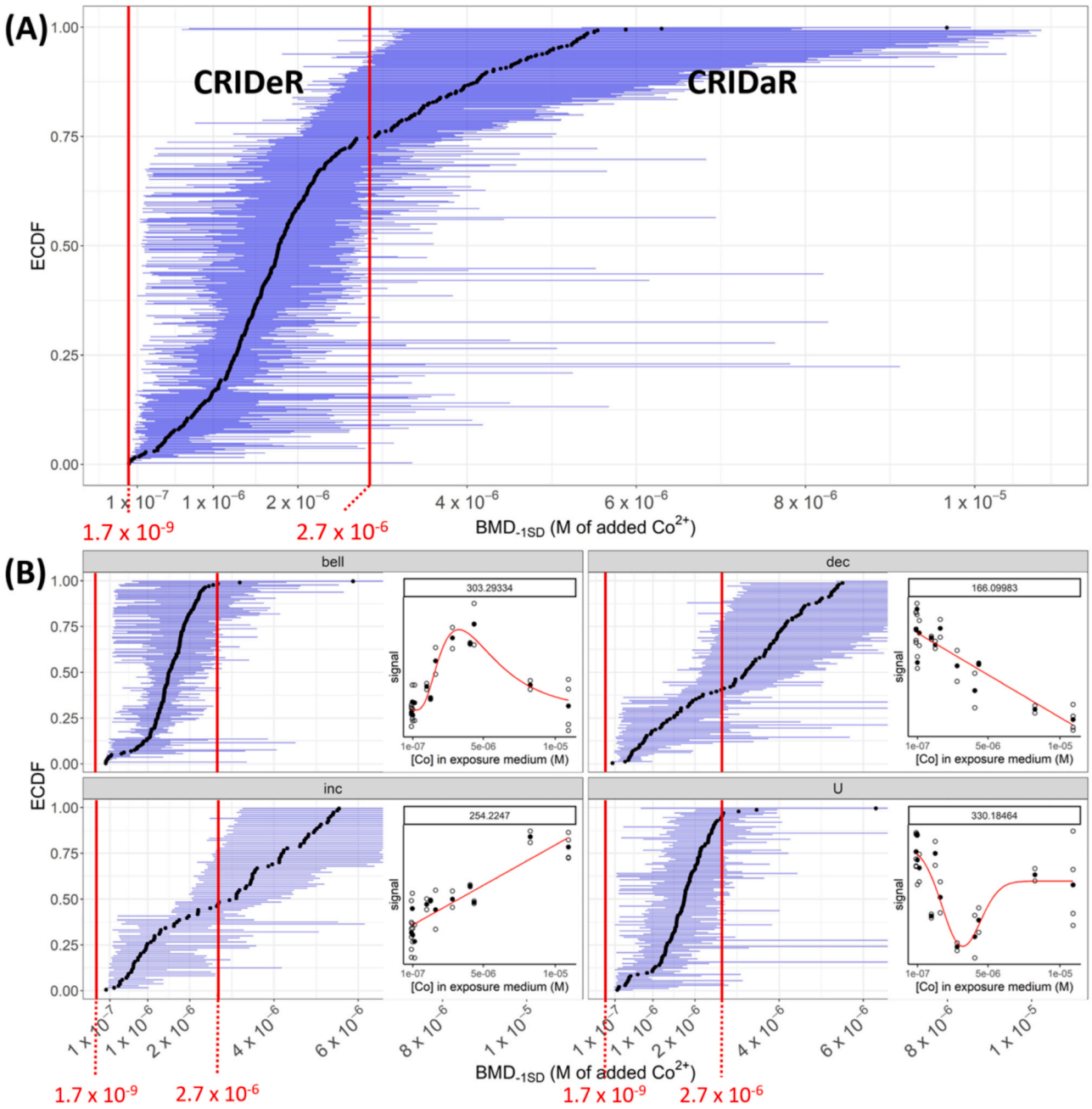

Fig. 5. Meta-metabolomics dose-response models of biofilms after 7 days of exposure to Co. (A) Distribution of $BMDs_{-1SD}$ as an ECDF (Empirical Cumulative Density Function) with 95% confidence intervals of each BMD_{-1SD} (M) in blue. (B) Distribution of $BMDs_{-1SD}$ as an ECDF split by trend of dose-response curves (bell: bell-shaped trend, dec: decreasing trend, inc: increasing trend and U: U-shaped trend) with 95% confidence intervals of each BMD_{-1SD} (M) in blue. The red lines correspond to the concentrations delimiting the suspected concentration ranges inducing defense and damage responses (CRIDeR and CRIDaR).

a significant effect implies that i) a large number of metabolites are affected and/or ii) the effect is greater than the control. Despite these challenges, a recent study successfully demonstrated a shift in biofilm meta-metabolome after only 15 min of exposure to 5 and 50 $\mu g \cdot L^{-1}$ diuron, an herbicide inhibiting the algal photosystem II [15]. The shift was shown to be concentration-dependent, with a higher number of metabolites affected at higher concentrations. The lack of a significant difference in the meta-metabolome response at D1 in our study might therefore be due to an exposure concentration to an essential metal that was too low to trigger a significant response in that short time scale. Statistical differences were, however, measured at D3 between the control and the two highest exposure concentrations. This is also the case at D7 between almost all treatments. Indeed, at that exposure time, a clear pattern was observed with an effect on meta-metabolome intensifying with increasing Co concentrations. All these responses were statistically different, except for the control and at 1×10^{-7} M Co. The change in the meta-metabolomic fingerprint of the biofilms depends thus both on the concentrations tested and the exposure time.

4.2. *Effect of Co on annotated metabolites*

Only a small part of the metabolomic fingerprint (7.5%) could be annotated, which is in line with the literature [18]. The use of the annotated metabolites provided similar results as a function of Co concentration and exposure time as those observed in the whole meta-metabolome analysis. Nevertheless, the annotated metabolites

provided insights on the cellular mechanisms modified by Co. The most noticeable effect observed on the annotated metabolites was the modification of the lipid contents (Fig. S3G and Fig. S3H). Specifically, increased levels of lipids and lipid precursors were observed. Several processes may explain these modifications: the formation of vacuoles made of lipid bilayers for metal sequestration [49], the repair of potential membrane damages caused by indirect oxidative stress [50], and the need for an additional internal source of energy in order to offset cellular and subcellular damage [51]. Finally, modifications of lipid profiles may also be due to a shift in microorganism community, as the variation in the meta-metabolome over time and the changes in pigment compositions might suggest (Fig. 2D) [52]. Recent studies combining the analysis of metagenomics and meta-metabolomics have demonstrated a change in the lipid profiles and taxa composition of stressed biofilms exposed to erythromycin and silver nanoparticles, although the biofilm microbial diversity was not altered [16,53]. Overall, our results add up to those highlighting the modification of the biofilm lipid contents when exposed to contaminants [15,16,54].

4.3. Comparison of meta-metabolomic response using the BMD_{-1SD} approach with the other measured biological parameters

In order to make full use of our chemical signal analysis without being limited by the annotation step, $BMDs_{-1SD}$ were derived from the dose-response curves constructed for each selected untargeted meta-metabolomic feature (Fig. 1). Within the range of tested Co concentrations, the use of $BMDs_{-1\ SD}$ highlighted that 78% of the untargeted meta-metabolomic features had their response modified between 1×10^{-6} and 5×10^{-6} M Co at D7 (Fig. 5A). Effects on chlorophyll pigments and biomass were in good agreement with this result. Indeed, Co effect was also observed to intensify between 1×10^{-6} and 5×10^{-6} M for both biological parameters (Fig. 2B and Fig. 2C). At D3, 53% of untargeted meta-metabolomic features already had their response modified between 1×10^{-6} and 5×10^{-6} M (Fig. S6). At the first sampling time, untargeted meta-metabolomic feature responses are statistically less numerous, as they are less significant. The accumulation of each untargeted meta-metabolomic feature response over time means that these significance thresholds are exceeded after D3 and even more so after D7.

The approach for detecting the effects of stressor via the use of BMDs was first used in toxicology to address the limits of predictors such as the effective concentration (EC_x), no observed adverse effect level or the lowest-observed adverse effect level, and to harmonise these predictive models of critical dose [55,56]. The BMDs approach is also gaining interest in ecotoxicology [57]. Indeed, the use of BMDs offer several advantages [58–60], *e.g.*, they (i) take into account the uncertainty related to the experiment and the inter-individual variability; (ii) consider the entire dose-response relationship; (iii) have a high precautionary principle; and (iv) associate a risk with each dose tested. In the present study, the results observed via the use of $BMDs_{-1SD}$ (Fig. 5A) are in good agreement with other biological parameters (biomass and chlorophyll content) despite being retrieved from predictive models (Fig. 2B and Fig. 2C).

A freshwater species sensitivity distribution for chronic Co exposure provided median hazardous concentrations for 5% of the community of 3.1×10^{-8} M based on EC_{10} values and 1.2×10^{-7} M using EC_{20} values [61]. In our study, for both values, no effect on the biomass and the chlorophyll contents were observed in biofilms (Fig. 2B, Fig. 2C and Fig. 2D) and the biofilm meta-metabolomic fingerprints were similar to those of the control at 10^{-7} M (Fig. 4 and Fig. S3). The 5% hazardous concentration based on the ECDF of biofilm untargeted meta-metabolomic features was 1.1×10^{-7} M at D3 and 4.1×10^{-7} M at D7, suggesting that our results are in line with those of Stubblefield et al. [61].

4.4. Using trends of dose-response curves to identify biofilm response to Co

The analysis of Co effect on biofilm meta-metabolome via the calculation of $BMDs_{-1SD}$ and the use of ECDF made it possible to distinguish, based on its inflection point, two distinct Co concentration ranges according to the meta-metabolomic dose-response at D7 (Fig. 5B). Range 1 (1.7×10^{-9} to 2.7×10^{-6} M of added Co^{2+}) was comprised mainly of untargeted meta-metabolomic features describing bell- or U-shaped dose-response models. In other studies, both bell- or U-shaped trends correspond to those of well-known defense biomarkers [23] such as antioxidant enzymes [24,62–64]. For example, in microalgae, catalase and superoxide dismutase activities were found to respond to Cd exposure in a bell-shaped manner [24]. Within range 1, the microorganisms would set up their defense mechanisms in order to counter the increase in intracellular Co content and its potential harmful effects (Fig. 2A and Fig. S2). We have defined this process as CRIDeR. Within range 2 (concentrations above 2.7×10^{-6} M of added Co^{2+}), the untargeted meta-metabolomic features presenting significant response exhibited mainly increasing or decreasing trends. These trends would thus describe the microorganism cellular state when defense mechanisms are overwhelmed and molecular or cellular damages are occurring [23]. In that range, damage biomarkers are commonly observed [24,65–68]. For example, malondialdehyde contents resulting from lipid peroxidation increase proportionally to Cu, Zn and Cd concentrations in microalgae [27,69]. Conversely, the contents of photosynthetic pigments decreased proportionally with Cr and Cd concentrations [69,70]. We have defined this process as CRIDaR. For Co, the identified threshold value of 2.7×10^{-6} M, which might separate CRIDeR and CRIDaR, is coherent with the changes observed using the traditional biological parameters studied here. Indeed, biofilm biomass decreased slightly at 1×10^{-6} M and much more significantly at 5×10^{-6} and 1×10^{-5} M (Fig. 2B). The effect of Co on the chlorophyll content strongly changed between 1×10^{-6} and 5×10^{-6} M (Fig. 2C). This CRIDaR threshold of 2.7×10^{-6} M is in good agreement with studies highlighting the harmful effects of Co on microalgae at the μM level [71,72]. The CRIDeR threshold was similar at D3, with a value of 2.1×10^{-6} M of added Co^{2+} (Fig. S6). Characterizing CRIDeR and CRIDaR can therefore determine the stress condition of the biofilm exposed to Co.

5. Conclusion

In this study, we have proposed a new approach to assessing the effects of metals on river biofilms. This is based on the use of the meta-metabolomic fingerprint obtained through an untargeted metabolomics analysis, which has the advantage of not having any initial a priori on the type of molecules (family or function) involved. This broadens the number of compounds potentially affected, compared with a targeted metabolomics approach (Fig. S1). In order to be able to use the entire chemical signal obtained with untargeted metabolomics and the information it contains, we have built dose-response models for each untargeted meta-metabolomic feature to extract $BMDs_{-1SD}$, subsequently aggregated in an ECDF. This ECDF highlighted two major concentration ranges in the metabolic response of biofilms based on dose-response curve trends: a CRIDeR and a CRIDaR. We then postulated that, from 2.7×10^{-6} M of added Co^{2+}, biofilm defense mechanisms were overcome and damage responses appeared. These results were in agreement with those obtained for biomass and chlorophyll *a* content. This promising, holistic approach nevertheless requires further development and validation, in particular to determine the influence of the choice of tested concentrations on the modeling of the distribution of the response of untargeted meta-metabolomic features and the characterization of curve trends.

The interpretation of trends for untargeted meta-metabolomic features dose-response models made it thus possible to identify and differentiate a CRIDeR and a CRIDaR, providing information on the level

of biofilm responses to a stress induced by Co. We have chosen to give these general terms of concentration ranges inducing defense or damage responses and not be specific to metabolites to leave open the possibility of testing this concept with other omics studies (transcriptomics, proteomics, etc.). It would also be possible to test this interpretation with the effect of exposure time and verify whether the time range inducing defense responses and time range inducing damage responses concept would also be applicable. Today, as ecotoxicologists, it seems important and necessary to try to make use of the entire set of metabolites available in the community. This novel approach is a promising avenue to improve the ecological risk assessment of contaminants and will generate new knowledge to go beyond using only one specific molecular biomarker at a time in ecotoxicological studies.

Associated content

Description of the biofilm colonization and the Co exposure in microcosms, the water analyses, Co speciation, total and intracellular Co concentrations, chlorophyll contents and meta-metabolomics analyses, and the detailed results of the physicochemical parameters of the river water and microcosms, the metal bioaccumulation, the effect of Co on annotated metabolites and the different parameters of the ECDF.

Environmental implication

Assessing the level of stress induced by a contaminant on a microorganism community is a challenging task compared to studies involving a single species. Here, we propose an original approach based on untargeted metabolomic response that includes both annotated and unannotated metabolites. This novel data processing method uses the trends of untargeted meta-metabolite dose-response curves to identify concentration ranges of defense and damage responses of biofilms exposed to cobalt. These results open up a new way of interpreting omics data using the whole chemical signal without being restricted by annotation and a new tool for environmental risk assessment.

Funding

This research was funded by the Research Partnership Chair E2S-UPPA-TotalEnergies-Rio Tinto (ANR-16-IDEX-0002).

CRediT authorship contribution statement

Simon Colas: Writing – review & editing, Writing – original draft, Visualization, Validation, Software, Methodology, Investigation, Formal analysis, Data curation, Conceptualization. **Benjamin Marie:** Writing – review & editing, Visualization, Software, Investigation, Formal analysis, Data curation. **Mathieu Milhe-Poutingon:** Investigation, Formal analysis. **Marie-Claire Lot:** Writing – review & editing. **Amiel Boullemant:** Writing – review & editing, Resources, Funding acquisition. **Claude Fortin:** Writing – review & editing, Supervision. **Séverine Le Faucheur:** Writing – review & editing, Writing – original draft, Validation, Supervision, Resources, Project administration, Investigation, Funding acquisition, Conceptualization.

Declaration of Competing Interest

The authors declare that they have no known competing financial interests or personal relationships that could have appeared to influence the work reported in this paper.

Data availability

Data will be made available on request.

Acknowledgments

We would like to thank the members of the *Pôle Environment & Développement Durable, Pôle d'Etudes et de Recherche de Lacq* for access to the TotalEnergies facilities for microcosms exposure and the UMR 7245 MCAM, the *Muséum national d'Histoire naturelle*, Paris, France, especially the *Cyanobactéries, Cyanotoxines et Environnement* team and the *Plateau technique de spectrométrie de masse bio-organique* for access to laboratories and technical facilities for the meta-metabolomics analyses. We also thank Patrick Baldoni-Andrey (TotalEnergies) and Nick Gurieff (Rio Tinto) for the stimulating scientific discussions. Special thanks to Scott Hepditch (Institut National de la Recherche Scientifique – Eau Terre Environnement, Québec, Canada) for his language assistance.

Appendix A. Supporting information

Supplementary data associated with this article can be found in the online version at doi:10.1016/j.jhazmat.2024.134099.

References

[1] Meylan, S., Behra, R., Sigg, L., 2003. Accumulation of copper and zinc in periphyton in response to dynamic variations of metal speciation in freshwater. Environ Sci Technol 37, 5204–5212. https://doi.org/10.1021/es034566+.
[2] Lavoie, I., Lavoie, M., Fortin, C., 2012. A mine of information: benthic algal communities as biomonitors of metal contamination from abandoned tailings. Sci Total Environ 425, 231–241. https://doi.org/10.1016/j.scitotenv.2012.02.057.
[3] Laderriere, V., Paris, L.-E., Fortin, C., 2020. Proton competition and free ion activities drive cadmium, copper, and nickel accumulation in river biofilms in a nordic ecosystem. Environments 7, 112. https://doi.org/10.3390/environments7120112.
[4] Barranguet, C., Greijdanus, M., Sinke, J.J., Admiraal, W., 2003. Copper-induced modifications of the modifications of the trophic relations in riverine algal-bacterial biofilms. Environ Toxicol Chem 22, 1340–1349. https://doi.org/10.1002/etc.5620220622.
[5] Bonet, B., Corcoll, N., Acuña, V., Sigg, L., Behra, R., Guasch, H., 2013. Seasonal changes in antioxidant enzyme activities of freshwater biofilms in a metal polluted Mediterranean stream. Sci Total Environ 444, 60–72. https://doi.org/10.1016/j.scitotenv.2012.11.036.
[6] Duong, T.T., Morin, S., Coste, M., Herlory, O., Feurtet-Mazel, A., Boudou, A., 2010. Experimental toxicity and bioaccumulation of cadmium in freshwater periphytic diatoms in relation with biofilm maturity. Sci Total Environ 408, 552–562. https://doi.org/10.1016/j.scitotenv.2009.10.015.
[7] Lavoie, M., Fortin, C., Campbell, P.G.C., 2012. Influence of essential elements on cadmium uptake and toxicity in a unicellular green alga: the protective effect of trace zinc and cobalt concentrations. Environ Toxicol Chem 31, 1445–1452. https://doi.org/10.1002/etc.1855.
[8] Morin, S., Duong, T.T., Herlory, O., Feurtet-Mazel, A., Coste, M., 2008. Cadmium toxicity and bioaccumulation in freshwater biofilms. Arch Environ Contam Toxicol 54, 173–186. https://doi.org/10.1007/s00244-007-9022-4.
[9] Morin, S., Lambert, A.S., Rodriguez, E.P., Dabrin, A., Coquery, M., Pesce, S., 2017. Changes in copper toxicity towards diatom communities with experimental warming. J Hazard Mater 334, 223–232. https://doi.org/10.1016/j.jhazmat.2017.04.016.
[10] Doose, C., Fadhlaoui, M., Morin, S., Fortin, C., 2021. Thorium exposure drives fatty acid and metal transfer from biofilms to the grazer *Lymnaea* sp. Environ Toxicol Chem 40, 2220–2228. https://doi.org/10.1002/etc.5067.
[11] Gauthier, L., Tison-Rosebery, J., Morin, S., Mazzella, N., 2020. Metabolome response to anthropogenic contamination on microalgae: a review. Metabolomics 16, 8. https://doi.org/10.1007/s11306-019-1628-9.
[12] Arora, N., Dubey, D., Sharma, M., Patel, A., Guleria, A., Pruthi, P.A., Kumar, D., Pruthi, V., Poluri, K.M., 2018. NMR-based metabolomic approach to elucidate the differential cellular responses during mitigation of arsenic(III, V) in a green microalga. ACS Omega 3, 11847–11856. https://doi.org/10.1021/acsomega.8b01692.
[13] Rocchetta, I., Mazzuca, M., Conforti, V., Ruiz, L., Balzaretti, V., de Molina, M. del C.R., 2006. Effect of chromium on the fatty acid composition of two strains of *Euglena gracilis*. Environ Pollut 141, 353–358. https://doi.org/10.1016/j.envpol.2005.08.035.
[14] Zhang, W., Tan, N.G.J., Li, S.F.Y., 2014. NMR-based metabolomics and LC-MS/MS quantification reveal metal-specific tolerance and redox homeostasis in *Chlorella vulgaris*. Mol Biosyst 10, 149–160. https://doi.org/10.1039/c3mb70425d.
[15] Creusot, N., Chaumet, B., Eon, M., Mazzella, N., Moreira, A., Morin, S., 2022. Metabolomics insight into the influence of environmental factors in responses of freshwater biofilms to the model herbicide diuron. Environ Sci Pollut Res 29, 29332–29347. https://doi.org/10.1007/s11356-021-17072-7.
[16] Pu, Y., Pan, J., Yao, Y., Ngan, W.Y., Yang, Y., Li, M., Habimana, O., 2021. Ecotoxicological effects of erythromycin on a multispecies biofilm model, revealed by metagenomic and metabolomic approaches. Environ Pollut 276, 116737. https://doi.org/10.1016/j.envpol.2021.116737.

[17] da Silva, R.R., Dorrestein, P.C., Quinn, R.A., 2015. Illuminating the dark matter in metabolomics. Proc Natl Acad Sci 112, 12549–12550. https://doi.org/10.1073/pnas.151687811.
[18] Dias, D., Jones, O., Beale, D., Boughton, B., Benheim, D., Kouremenos, K., Wolfender, J.-L., Wishart, D., 2016. Current and future perspectives on the structural identification of small molecules in biological systems. Metabolites 6, 46. https://doi.org/10.3390/metabo6040046.
[19] Godzien, J., Gil de la Fuente, A., Otero, A., Barbas, C., 2018. Metabolite annotation and identification. in: Compr. Anal. Chem. Elsevier, pp. 415–445. https://doi.org/10.1016/bs.coac.2018.07.004.
[20] Larras, F., Billoir, E., Baillard, V., Siberchicot, A., Scholz, S., Wubet, T., Tarkka, M., Schmitt-Jansen, M., Delignette-Muller, M.-L., 2018. DRomics: a turnkey tool to support the use of the dose–response framework for omics data in ecological risk assessment. Environ Sci Technol 52, 14461–14468. https://doi.org/10.1021/acs.est.8b04752.
[21] EFSA Scientific Committee, Hardy, A., Benford, D., Halldorsson, T., Jeger, M.J., Knutsen, K.H., More, S., Mortensen, A., Naegeli, H., Noteborn, H., Ockleford, C., Ricci, A., Rychen, G., Silano, V., Solecki, R., Turck, D., Aerts, M., Bodin, L., Davis, A., Edler, L., Gundert-Remy, U., Sand, S., Slob, W., Bottex, B., Abrahantes, J. C., Marques, D.C., Kass, G., Schlatter, J.R., 2017. Update: use of the benchmark dose approach in risk assessment. EFSA J 15. https://doi.org/10.2903/j.efsa.2017.4658.
[22] Larras, F., Billoir, E., Scholz, S., Tarkka, M., Wubet, T., Delignette-Muller, M.-L., Schmitt-Jansen, M., 2020. A multi-omics concentration-response framework uncovers novel understanding of triclosan effects in the chlorophyte *Scenedesmus vacuolatus*. J Hazard Mater 397, 122727. https://doi.org/10.1016/j.jhazmat.2020.122727.
[23] Colas, S., Le Faucheur, S., 2024. How do biomarkers dance? Specific moves of defense and damage biomarkers for biological interpretation of dose-response model trends. J Hazard Mater 465, 133180. https://doi.org/10.1016/j.jhazmat.2023.133180.
[24] Cheng, J., Qiu, H., Chang, Z., Jiang, Z., Yin, W., 2016. The effect of cadmium on the growth and antioxidant response for freshwater algae *Chlorella vulgaris*. SpringerPlus 5, 1290. https://doi.org/10.1186/s40064-016-2963-1.
[25] Ran, X., Liu, R., Xu, S., Bai, F., Xu, J., Yang, Y., Shi, J., Wu, Z., 2015. Assessment of growth rate, chlorophyll *a* fluorescence, lipid peroxidation and antioxidant enzyme activity in *Aphanizomenon flos-aquae*, *Pediastrum simplex* and *Synedra acus* exposed to cadmium. Ecotoxicology 24, 468–477. https://doi.org/10.1007/s10646-014-1395-3.
[26] Navarrete, A., González, A., Gómez, M., Contreras, R.A., Díaz, P., Lobos, G., Brown, M.T., Sáez, C.A., Moenne, A., 2019. Copper excess detoxification is mediated by a coordinated and complementary induction of glutathione, phytochelatins and metallothioneins in the green seaweed *Ulva compressa*. Plant Physiol Biochem 135, 423–431. https://doi.org/10.1016/j.plaphy.2018.11.019.
[27] Li, M., Hu, C., Zhu, Q., Chen, L., Kong, Z., Liu, Z., 2006. Copper and zinc induction of lipid peroxidation and effects on antioxidant enzyme activities in the microalga *Pavlova viridis* (Prymnesiophyceae). Chemosphere 62, 565–572. https://doi.org/10.1016/j.chemosphere.2005.06.029.
[28] Davis, J.M., Svendsgaard, D.J., 1990. U-Shaped dose-response curves: their occurrence and implications for risk assessment. J Toxicol Environ Health 30, 71–83. https://doi.org/10.1080/15287399009531412.
[29] Swenberg, J.A., Fryar-Tita, E., Jeong, Y.-C., Boysen, G., Starr, T., Walker, V.E., Albertini, R.J., 2008. Biomarkers in toxicology and risk assessment: informing critical dose–response relationships. Chem Res Toxicol 21, 253–265. https://doi.org/10.1021/tx700408t.
[30] U.S. Geological Survey, 2010. Mineral commodity summaries 2010. U.S. Geological Survey. https://doi.org/10.3133/mineral2010.
[31] U.S. Geological Survey, 2020. Mineral commodity summaries 2020. U.S. Geological Survey. https://doi.org/10.3133/mcs2020.
[32] Institut national de l'environnement industriel et des risques, Substances Pertinentes à Surveiller (SPAS) dans les eaux de surface - Etude des données à l'échelle des bassins hydrographiques et selon les types de pression chimique, Ineris, Verneuil-en-Halatte, 2022. ⟨https://www.ineris.fr/fr/substances-pertinentes-surveiller-spas-eaux-surface-etude-donnees-echelle-bassins-hydrographiques⟩ (accessed June 2, 2023).
[33] Canada Gazette, Order Adding a Toxic Substance to Schedule 1 to the Canadian Environmental Protection Act, 1999: SOR/2019–197, 2019. ⟨https://gazette.gc.ca/rp-pr/p2/2019/2019–06-26/html/sor-dors197-eng.html⟩ (accessed June 2, 2023).
[34] Barrio-Parra, F., Elío, J., De Miguel, E., García-González, J.E., Izquierdo, M., Álvarez, R., 2018. Environmental risk assessment of cobalt and manganese from industrial sources in an estuarine system. Environ Geochem Health 40, 737–748. https://doi.org/10.1007/s10653-017-0020-9.
[35] Bhutiani, R., Kulkarni, D.B., Khanna, D.R., Gautam, A., 2017. Geochemical distribution and environmental risk assessment of heavy metals in groundwater of an industrial area and its surroundings, Haridwar, India. Energy Ecol Environ 2, 155–167. https://doi.org/10.1007/s40974-016-0019-6.
[36] Khan, Z.I., Arshad, N., Ahmad, K., Nadeem, M., Ashfaq, A., Wajid, K., Bashir, H., Munir, M., Huma, B., Memoona, H., Sana, M., Nawaz, K., Sher, M., Abbas, T., Ugulu, I., 2019. Toxicological potential of cobalt in forage for ruminants grown in polluted soil: a health risk assessment from trace metal pollution for livestock. Environ Sci Pollut Res 26, 15381–15389. https://doi.org/10.1007/s11356-019-04959-9.
[37] Xu, F., Wang, Y., Chen, X., Liang, L., Zhang, Y., Zhang, F., Zhang, T., 2022. Assessing the environmental risk and mobility of cobalt in sediment near nonferrous metal mines with risk assessment indexes and the diffusive gradients in thin films (DGT) technique. Environ Res 212, 113456. https://doi.org/10.1016/j.envres.2022.113456.
[38] Olguín, E.J., Sánchez-Galván, G., 2012. Heavy metal removal in phytofiltration and phycoremediation: the need to differentiate between bioadsorption and bioaccumulation. N Biotechnol 30, 3–8. https://doi.org/10.1016/j.nbt.2012.05.020.
[39] Jeffrey, S.W., Humphrey, G.F., 1975. New spectrophotometric equations for determining chlorophylls *a*, *b*, c_1 and c_2 in higher plants, algae and natural phytoplankton. Biochem Physiol Pflanz 167, 191–194. https://doi.org/10.1016/S0015-3796(17)30778-3.
[40] Le Moigne, D., Demay, J., Reinhardt, A., Bernard, C., Kim Tiam, S., Marie, B., 2021. Dynamics of the metabolome of *Aliinostoc* sp. PMC 882.14 in response to light and temperature variations. Metabolites 11, 745. https://doi.org/10.3390/metabo11110745.
[41] Sud, M., Fahy, E., Cotter, D., Azam, K., Vadivelu, I., Burant, C., Edison, A., Fiehn, O., Higashi, R., Nair, K.S., Sumner, S., Subramaniam, S., 2016. Metabolomics Workbench: An international repository for metabolomics data and metadata, metabolite standards, protocols, tutorials and training, and analysis tools. Nucleic Acids Res 44, D463–D470. https://doi.org/10.1093/nar/gkv1042.
[42] Leguay, S., Lavoie, I., Levy, J.L., Fortin, C., 2016. Using biofilms for monitoring metal contamination in lotic ecosystems: The protective effects of hardness and pH on metal bioaccumulation: Monitoring metal contamination using stream biofilms. Environ Toxicol Chem 35, 1489–1501. https://doi.org/10.1002/etc.3292.
[43] Niederer, C., Behra, R., Harder, A., Schwarzenbach, R.P., Escher, B.I., 2004. Mechanistic approaches for evaluating the tocicity of reactive organochlorines and epoxides in green algae. Environ Toxicol Chem 23, 697. https://doi.org/10.1897/03-83.
[44] Yu, X., Jin, X., Liu, H., Yu, Y., Tang, J., Zhou, R., Yin, A., Sun, J., Zhu, L., 2023. Enhanced degradation of atrazine through UV/bisulfite: mechanism, reaction pathways and toxicological analysis. Sci Total Environ 856, 159157. https://doi.org/10.1016/j.scitotenv.2022.159157.
[45] Morelli, E., Scarano, G., 2001. Synthesis and stability of phytochelatins induced by cadmium and lead in the marine diatom *Phaeodactylum tricornutum*. Mar Environ Res 52, 383–395. https://doi.org/10.1016/S0141-1136(01)00093-9.
[46] Morelli, E., Scarano, G., 2004. Copper-induced changes of non-protein thiols and antioxidant enzymes in the marine microalga *Phaeodactylum tricornutum*. Plant Sci 167, 289–296. https://doi.org/10.1016/j.plantsci.2004.04.001.
[47] Liu, W., Majumdar, S., Li, W., Keller, A.A., Slaveykova, V.I., 2020. Metabolomics for early detection of stress in freshwater alga *Poterioochromonas malhamensis* exposed to silver nanoparticles. Sci Rep 10, 20563. https://doi.org/10.1038/s41598-020-77521-0.
[48] Slaveykova, V.I., Majumdar, S., Regier, N., Li, W., Keller, A.A., 2021. Metabolomic responses of green alga *Chlamydomonas reinhardtii* exposed to sublethal concentrations of inorganic and methylmercury. Environ Sci Technol 55, 3876–3887. https://doi.org/10.1021/acs.est.0c08416.
[49] Nishikawa, K., Yamakoshi, Y., Uemura, I., Tominaga, N., 2003. Ultrastructural changes in *Chlamydomonas acidophila* (Chlorophyta) induced by heavy metals and polyphosphate metabolism. FEMS Microbiol Ecol 44, 253–259. https://doi.org/10.1016/S0168-6496(03)00049-7.
[50] Zhang, S., He, Y., Sen, B., Wang, G., 2020. Reactive oxygen species and their applications toward enhanced lipid accumulation in oleaginous microorganisms. Bioresour Technol 307, 123234. https://doi.org/10.1016/j.biortech.2020.123234.
[51] Popko, J., 2016. Lipid composition of *Chlamydomonas reinhardtii*. In: Wenk, M.R. (Ed.), Encycl. Lipidomics. Springer Netherlands, Dordrecht, pp. 1–6. https://doi.org/10.1007/978-94-007-7864-1_126-1.
[52] Fadhlaoui, M., Laderriere, V., Lavoie, I., Fortin, C., 2020. Influence of temperature and nickel on algal biofilm fatty acid composition. Environ Toxicol Chem 39, 1566–1577. https://doi.org/10.1002/etc.4741.
[53] Yang, P., Pan, J., Wang, H., Xiaohan, X., Zeling, X., Chen, X., Yang, Y., Sun, H., Li, M., Habimana, O., 2023. Structural, metagenomic and metabolic shifts in multispecies freshwater biofilm models exposed to silver nanoparticles. J Environ Chem Eng 11, 109162. https://doi.org/10.1016/j.jece.2022.109162.
[54] Favre, L., Ortalo-Magné, A., Kerloch, L., Pichereaux, C., Misson, B., Briand, J.-F., Garnier, C., Culioli, G., 2019. Metabolomic and proteomic changes induced by growth inhibitory concentrations of copper in the biofilm-forming marine bacterium *Pseudoalteromonas lipolytica*. Metallomics 11, 1887–1899. https://doi.org/10.1039/C9MT00184K.
[55] Crump, K.S., 1984. A new method for determining allowable daily intakes, Toxicol. Sci, 4, 854–871. https://doi.org/10.1016/0272-0590(84)90107-6.
[56] Gaylor, D., Ryan, L., Krewski, D., Zhu, Y., 1998. Procedures for calculating benchmark doses for health risk assessment. Regul Toxicol Pharmacol 28, 150–164. https://doi.org/10.1006/rtph.1998.1247.
[57] Mayfield, D.B., Skall, D.G., 2018. Benchmark dose analysis framework for developing wildlife toxicity reference values: BMD analysis framework for wildlife TRVs. Environ Toxicol Chem 37, 1496–1508. https://doi.org/10.1002/etc.4082.
[58] Bokkers, B.G.H., Slob, W., 2005. A comparison of ratio distributions based on the NOAEL and the benchmark approach for subchronic-to-chronic extrapolation. Toxicol Sci 85, 1033–1040. https://doi.org/10.1093/toxsci/kfi144.
[59] Bokkers, B.G.H., Slob, W., 2007. Deriving a data-based interspecies assessment factor using the NOAEL and the benchmark dose approach. Crit Rev Toxicol 37, 355–373. https://doi.org/10.1080/10408440701249224.
[60] Bonvallot, N., Bodin, L., Duboudin, C., Bard, D., 2009. Benchmark dose: définitions, intérêt et usages en évaluation des risques sanitaires. Environ Risqu– St 8, 529–537.
[61] Stubblefield, W.A., Van Genderen, E., Cardwell, A.S., Heijerick, D.G., Janssen, C.R., De Schamphelaere, K.A.C., 2020. Acute and chronic toxicity of cobalt to freshwater

organisms: Using a Species Sensitivity Distribution approach to establish international water quality standards. Environ Toxicol Chem 39, 799–811. https://doi.org/10.1002/etc.4662.

[62] Bártová, K., Hilscherová, K., Babica, P., Maršálek, B., Bláha, L., 2011. Effects of microcystin and complex cyanobacterial samples on the growth and oxidative stress parameters in green alga *Pseudokirchneriella subcapitata* and comparison with the model oxidative stressor-herbicide paraquat. Environ Toxicol 26, 641–648. https://doi.org/10.1002/tox.20601.

[63] Hong, Y., Tan, Y., Meng, Y., Yang, H., Zhang, Y., Warren, A., Li, J., Lin, X., 2017. Evaluation of biomarkers for ecotoxicity assessment by dose-response dynamic models: Effects of nitrofurazone on antioxidant enzymes in the model ciliated protozoan *Euplotes vannus*. Ecotoxicol Environ Saf 144, 552–559. https://doi.org/10.1016/j.ecoenv.2017.06.069.

[64] Abassi, S., Wang, H., Ponmani, T., Ki, J., 2019. Small heat shock protein genes of the green algae *Closterium ehrenbergii*: Cloning and differential expression under heat and heavy metal stresses. Environ Toxicol 34, 1013–1024. https://doi.org/10.1002/tox.22772.

[65] Nie, X., Wang, X., Chen, J., Zitko, V., An, T., 2008. Response of the freshwater alga *Chlorella vulgaris* to trichloroisocyanuric acid and ciprofloxacin. Environ Toxicol Chem 27, 168. https://doi.org/10.1897/07-028.1.

[66] Melegari, S.P., Perreault, F., Costa, R.H.R., Popovic, R., Matias, W.G., 2013. Evaluation of toxicity and oxidative stress induced by copper oxide nanoparticles in the green alga *Chlamydomonas reinhardtii*. Aquat Toxicol 142–143, 431–440. https://doi.org/10.1016/j.aquatox.2013.09.015.

[67] Xiao, A., Wang, C., Chen, J., Guo, R., Yan, Z., Chen, J., 2016. Carbon and metal quantum dots toxicity on the microalgae *Chlorella pyrenoidosa*. Ecotoxicol Environ Saf 133, 211–217. https://doi.org/10.1016/j.ecoenv.2016.07.026.

[68] Fang, B., Shi, J., Qin, L., Feng, M., Cheng, D., Wang, T., Zhang, X., 2018. Toxicity evaluation of 4,4′-di-CDPS and 4,4′-di-CDE on green algae *Scenedesmus obliquus*: growth inhibition, change in pigment content, and oxidative stress. Environ Sci Pollut Res 25, 15630–15640. https://doi.org/10.1007/s11356-018-1749-0.

[69] Çelekli, A., Kapı, M., Bozkurt, H., 2013. Effect of cadmium on biomass, pigmentation, malondialdehyde, and proline of *Scenedesmus quadricauda* var. *longispina*. Bull Environ Contam Toxicol 91, 571–576. https://doi.org/10.1007/s00128-013-1100-x.

[70] Rai, U.N., Singh, N.K., Upadhyay, A.K., Verma, S., 2013. Chromate tolerance and accumulation in *Chlorella vulgaris* L.: Role of antioxidant enzymes and biochemical changes in detoxification of metals. Bioresour Technol 136, 604–609. https://doi.org/10.1016/j.biortech.2013.03.043.

[71] El-Din, S.M.M., 2016. Effects of heavy metals (copper, cobalt and lead) on the growth and photosynthetic pigments of the green alga *Chlorella pyrenoidosa* H. Chick. Catrina Int J Environ Sci 15, 1–10.

[72] Fawzy, M.A., Hifney, A.F., Adam, M.S., Al-Badaani, A.A., 2020. Biosorption of cobalt and its effect on growth and metabolites of *Synechocystis pevalekii* and *Scenedesmus bernardii*: isothermal analysis. Environ Technol Innov 19, 100953. https://doi.org/10.1016/j.eti.2020.100953.